

# van Hove singularity at the Fermi level due to oxygen in noble metal

Sudipta Roy Barman<sup>1</sup> and Aparna Chakrabarti<sup>2,3</sup>

<sup>1</sup>UGC-DAE Consortium for Scientific Research, Khandwa Road, Indore, 452001, Madhya Pradesh, India

<sup>2</sup>Theory and Simulations Laboratory, Raja Ramanna Centre for Advanced Technology, Indore, 452013, India and

<sup>3</sup>Homi Bhabha National Institute, Anushakti Nagar, Mumbai, 400094, India

The interaction of oxygen with noble metals such as silver has been an important topic of research for many decades. Here, we show the occurrence of a van Hove singularity manifested through a sharp peak in the density of states at the Fermi level when oxygen atoms occupy disordered substitutional positions in the close packed noble metal lattice of Ag, Au or Ag-Au alloy. The peak originates from the O  $2p$  states, and is related to a disorder broadened flat band that straddles almost all the high symmetry directions of the Brillouin zone. We argue that disordered oxygen bound mainly by the van der Waals force and stabilized by hybridization with the noble metal might be realized in nano-structures and lead to novel phenomena.

## Introduction:

From way back, the interaction of oxygen with noble metals such as silver has fascinated scientists through different intriguing phenomena such as high solubility of oxygen in liquid Ag that changes its freezing point[1], dissociation of oxygen molecule at the silver surface[2] and incorporation of oxygen atoms (O-atoms) in the bulk[3–6] enhancing its catalytic activity[7, 8], elongation of free standing silver atom chain by incorporation of alternate O-atoms[9], and anomalous superconducting proximity effect where Ag layer increases the transition temperature ( $T_C$ ) of Pb[10]. From density functional theory (DFT), Gravi $\acute{e}$ l *et al.* found that oxygen dissociates into chemisorbed atomic species with no barrier[2], while Li *et al.* showed that O-atoms in Ag are responsible for the catalysis[8]. From an experimental study, Bao *et al.* reported that incorporation of O-atoms in the subsurface causes a 3% expansion of the topmost layer[3]. Eberhart *et al.* performed a first-principles calculation of the charge density to find that O-atom transport through the octahedral interstitial sites is favored in Ag and Cu, but not in Au[4]. The authors however did not consider the vacancies, and a later DFT study showed that rather than existing as an O atom- vacancy pair, the O-atom prefers to occupy the Ag vacancy *i.e.* exist at the substitutional site[5]. Baird *et al.* proposed how an O-atom would diffuse in Ag by absorbing a phonon to overcome the potential energy barrier[6]. Among the different types of O-atoms that were identified,  $O_\beta$  is the bulk dissolved oxygen, while  $O_\gamma$  is a strongly bound species that diffuses in Ag[7]. The stoichiometric oxides of Ag are semiconducting and these have been studied by DFT primarily to understand why high  $T_C$  superconductivity is absent in Ag oxides in spite of their similarity with Cu oxides[11, 12].

Compared to the bulk, Ag nano-particles (NP) are more susceptible to oxidation[13, 14]. Large concentrations of O and C (0.55 and 5 times, respectively with respect to Ag) in Ag@Au core-shell particles, where Ag is the core and Au is the shell, have been reported from x-ray photoelectron spectroscopy (XPS)[14]. Significantly,

the oxygen and carbon signals increase as XPS is measured in the bulk sensitive mode, indicating that these are present primarily within the NP and not at the surface. A detailed work using x-ray absorption fine structure spectroscopy and molecular dynamics by Shibata *et al.* showed existence of vacancies in Au@Ag NP at room temperature that facilitates interface alloying[15]. A scanning tunneling microscopy study showed that with application of electrochemical potential, vacancy clusters can grow and diffuse on Ag-Au alloy[16]. Recently, Yue *et al.* have demonstrated by transmission electron microscopy and theoretical simulation that oxygen molecules dissociate on the surface of silver NP and diffuse through them to reach the silver/carbon interface and eventually oxidize the carbon[17].

In this work, we investigate how the electronic structure of fcc noble metals such as Ag and Au is modified by O-atoms in the disordered substitutional (*i.e.* O-atoms in metal vacancy positions) and interstitial positions using the spin polarized fully relativistic Korringa Kohn Rostoker (SPRKKR) method[18]. For O-atoms in the substitutional position, we find a huge increase in the density of states (DOS) at the Fermi level ( $E_F$ ) caused by a sharp peak related to O  $2p$ -like states. The Bloch spectral function, which is the counterpart of dispersion relation for an ordered solid, shows flat and narrow regions straddling the Fermi level along almost all the high symmetry directions of the Brillouin zone (BZ), similar to a flat band in an ordered solid. We show that this phenomenon also occurs in Au, as well as Ag-Au alloy. We hence argue that in nano-structures, presence of disordered oxygen bound by dispersive force and stabilized by the noble metal matrix might lead to novel phenomena such as superconductivity, as reported very recently[19].

## Methods:

We have performed self-consistent band structure calculations using SPRKKR method in the atomic sphere approximation[18] within the generalized gradient approximation[20]. The site disorder was treated by coherent potential approximation (CPA) that calculates the configurationally averaged electronic structure self

consistently within a mean-field theory. In general, CPA focuses on understanding the scattering of electrons in a material which exhibits spatial inhomogeneity and has turned out to be the most well established way of calculating the influence of disorder on the electronic properties of different materials. The angular momentum expansion up to  $l_{max} = 4$  has been used for each atom. The energy convergence criterion and CPA tolerance has been set to  $10^{-5}$  Ry. BZ integrations were performed on a  $45 \times 45 \times 45$  mesh of  $k$ -points in the irreducible wedge of the BZ. Spin polarized calculations were performed with small starting moments, but the converged result did not show any moment.

The supercell calculation with full potential linearized augmented plane wave method[27] has been performed with 8000  $k$  points in BZ (256  $k$  points in the irreducible BZ). The energy cut-off is about 14.5 Ry and the tolerance for energy convergence is  $10^{-4}$  Ry. The cohesive energy, which is the total energy of the constituent atoms minus the total energy of the compound, has been calculated using the full potential linearized augmented plane wave method. The total energies for the constituent atoms are calculated in a cubic box of size about 9 Å.

## Results and Discussion:

The total and partial density of states (PDOS) of Ag with different amounts of randomly substituted O-atoms are shown in Fig. 1(a-e). The calculations are performed using the equilibrium lattice constant ( $a_{eq}$ ) obtained by fitting the variation of the total energy as a function of lattice constant using a polynomial function (Fig. 2).

In all cases,  $a_{eq}$  turns out to be within a few percent of the Ag lattice constant (4.085Å). A broad hump centered around -0.7 eV in the total DOS of  $\text{Ag}_{88}\text{O}_{12}$  that is absent in Ag originates from the O  $2p$ -like states Fig. 1(a,b). This feature causes an enhancement of the DOS at  $E_F$  ( $n_F$ ) by 46% compared to Ag. The intensity of the hump increases in  $\text{Ag}_{75}\text{O}_{25}$ , and it shifts very close to  $E_F$  (-0.2 eV). It is striking to note that, for  $\text{Ag}_{60}\text{O}_{40}$ , this O  $2p$  related peak becomes narrower and appears exactly at  $E_F$ , causing a very large increase of  $n_F$  by 286% (Fig. 1(d,f)). This effect is even more pronounced for  $\text{Ag}_{50}\text{O}_{50}$ , with a whopping 400% increase of  $n_F$ , with the maximum of the O  $2p$  PDOS peak right at  $E_F$  (Fig. 1(e,f)). The enhancement of  $n_F$  is also obtained for Au-O (Fig. 1(h,i)), as well as in Ag-Au-O (Fig. 1(g,j)). In fact, for the same oxygen content,  $n_F$  is largest in Au-O (e.g.  $n_F = 1.37$  states/eV/atom for  $\text{Au}_{60}\text{O}_{40}$  in Fig. 1(i)), compared to  $n_F = 1.25$  states/eV/atom for  $\text{Au}_{30}\text{Ag}_{30}\text{O}_{40}$  in Fig. 1(j) and  $n_F = 1.07$  states/eV/atom for  $\text{Ag}_{60}\text{O}_{40}$  in Fig. 1(d)). For a disordered system, an equivalent of the band dispersion  $E(k)$  can be obtained through the Bloch spectral function,  $A_B(k, E)$ , which is defined as the Fourier transform of the retarded single electron Green's function[21]. For an ordered system, Bloch spectral function (BSF)

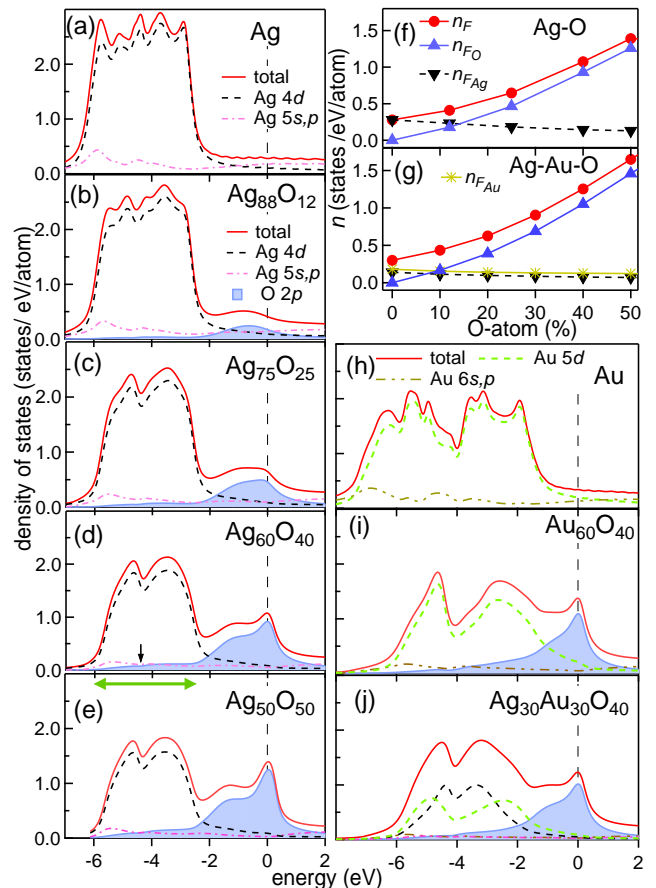


Figure 1: Total and partial density of states of (a) Ag, (b)  $\text{Ag}_{88}\text{O}_{12}$ , (c)  $\text{Ag}_{75}\text{O}_{25}$ , (d)  $\text{Ag}_{60}\text{O}_{40}$ , (e)  $\text{Ag}_{50}\text{O}_{50}$ , (h) Au, (i)  $\text{Au}_{60}\text{O}_{40}$ , and (j)  $\text{Ag}_{30}\text{Au}_{30}\text{O}_{40}$ . The total DOS at  $E_F$  ( $n_F$ ) and the total Ag ( $n_{F,Ag}$ ), O ( $n_{F,O}$ ) and Au ( $n_{F,Au}$ ) contributions to  $n_F$  for (f) Ag-O (g) Ag-Au-O, as a function of O-atom content.

reduces to a set of  $\delta$  functions at the band energies giving  $E(k)$ . With introduction of disorder, these  $\delta$ -function peaks are broadened. To find the origin of the DOS peak at  $E_F$  in Fig. 1, we have calculated the BSF along the high symmetry directions of the fcc BZ. If the BSF of  $\text{Ag}_{88}\text{O}_{12}$  in Fig. 3(b) is compared to  $E(k)$  of Ag (Fig. 3(a)), it is observed that the dispersing Ag  $s, p$  band with a kink at the  $L$  point splits in the former. The splitting happens because the occupied band shifts down in energy to about -1.5 eV, while the unoccupied part up to 1 eV diminishes in intensity (in Fig. 3(b) see the red colored band around  $L$  point, red is about 25 in the relative intensity logarithmic color scale with green as maximum ( $\approx 100$ ) and white as minimum (zero)). The same happens for the other dispersing Ag  $s-p$  bands, e.g. the bands crossing  $E_F$  at middle of  $\Delta-X$  and near  $M$  point. Thus, evidently, the contribution of Ag  $s-p$  states to  $n_F$  decreases. A curious observation from Fig. 3(b) is the appearance of states of low intensity at  $E_F$  (blue region,

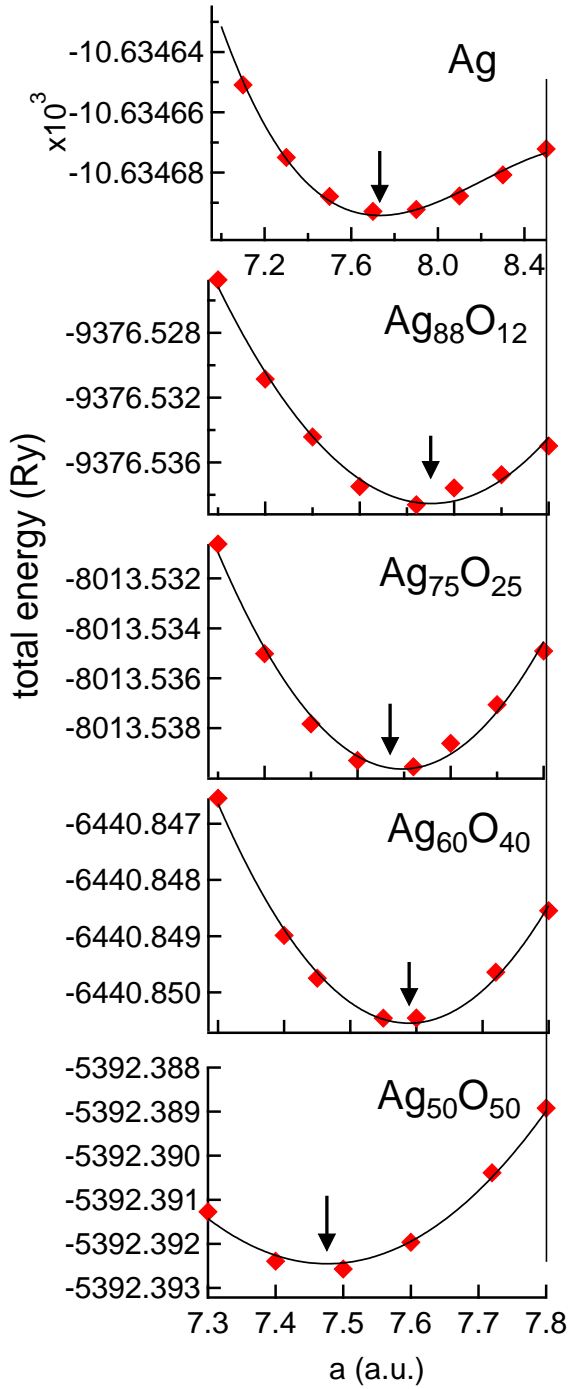


Figure 2: The total energy as a function of lattice constant  $a$  for different Ag-O compositions, the equilibrium lattice constant  $a_{eq}$  is indicated by black arrow.

5 in the intensity scale) and we examine how these evolve with larger O-atom content. Strikingly, for Ag<sub>75</sub>O<sub>25</sub> in Fig. 3(c), parts of the blue region become intense and appear as flat red bands along  $W-U$  and  $Q-\Sigma$  (encircled by white dashes). The flat band along  $Q-\Sigma$  connects two

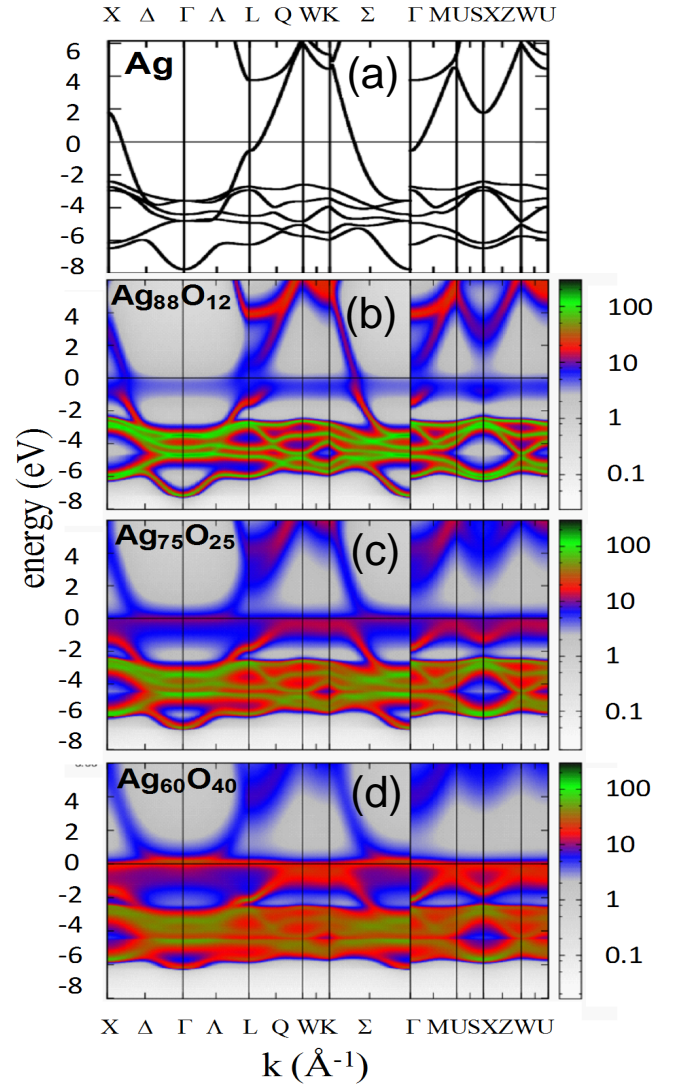


Figure 3: (a) The band dispersion  $E(k)$  along the different high symmetry directions of Ag compared with the Bloch spectral function  $A_B(k, E)$  along the same directions for (b) Ag<sub>75</sub>O<sub>25</sub>, and (c) Ag<sub>60</sub>O<sub>40</sub>, the color scale is shown on the right side.

dispersing bands crossing  $L$  and  $\Sigma$ . A parabolic band emerges with minimum at  $X$  at  $-1.5$  eV and disperses up to the flat band along  $W-U$  (encircled by white dashes). Weak flat bands (light red color) at  $E_F$  is also observed along  $\Delta-\Gamma-\Lambda$  and  $\Sigma-\Gamma$ . A spectacular effect occurs for Ag<sub>60</sub>O<sub>40</sub> (Fig. 3(d)): a flat narrow band (red color) appears at  $E_F$  spanning all the high symmetry directions from  $X-\Gamma-L-W-K-\Gamma$  and  $\Gamma-U-X-W-U$  that we have calculated (encircled by yellow dashes). The very wide  $k$  range of the flat band, as if it is ubiquitous, along the different directions of the fcc BZ is completely unique. Obviously, this is the origin of the sharp DOS peak at  $E_F$ . The intensity of this flat band further increases for

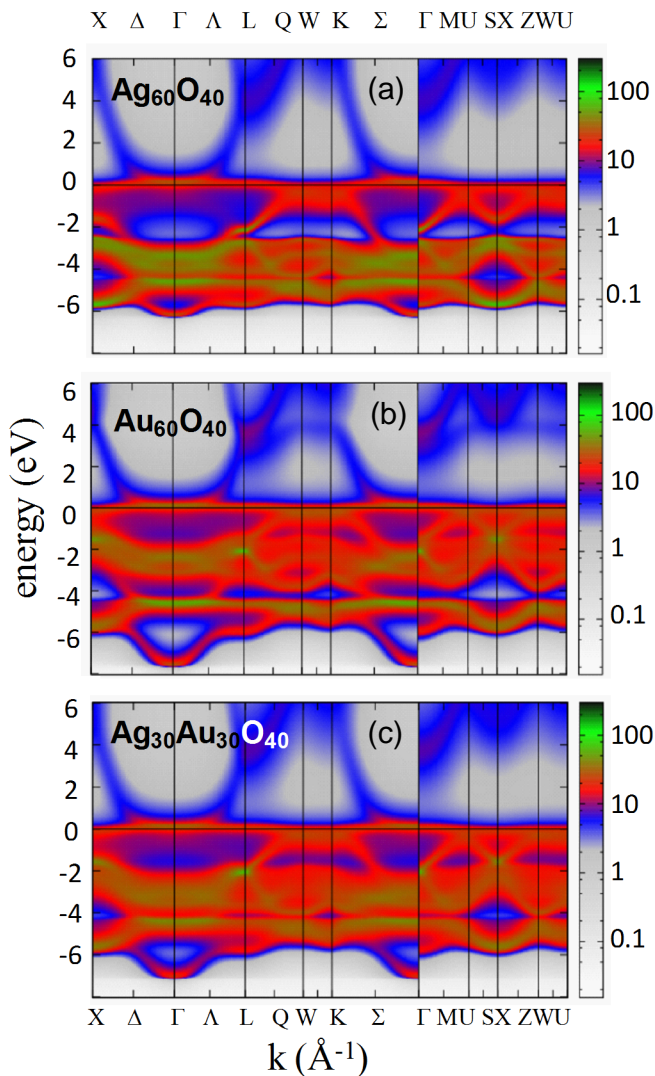


Figure 4: A comparison of the Bloch spectral function  $A_B(k, E)$  along the different high symmetry directions of the fcc BZ (a)  $\text{Ag}_{60}\text{O}_{40}$ , (b)  $\text{Au}_{60}\text{O}_{40}$ , and (c)  $\text{Ag}_{30}\text{Au}_{30}\text{O}_{40}$ ; the color scale is shown on the right side. The flat band at  $E_F$  is observed in all cases.

$\text{Ag}_{50}\text{O}_{50}$ . The BSF curves of  $\text{Au}_{60}\text{O}_{40}$  and  $\text{Au}_{30}\text{Ag}_{30}\text{O}_{40}$  also show presence of this intense flat band at  $E_F$  (Fig. 4). Thus, in analogy with an ordered solid where flat bands give rise to van Hove singularity, presence of flat bands obtained from the BSF establish existence of van Hove singularity at  $E_F$  in Ag/Au-O (Fig. 3, 4), albeit broadened by disorder. van Hove singularity at  $E_F$  is one of the crucial parameters that determines the superconducting energy gap and  $T_C$  of a superconductor [22–24] and observation of such an effect could open up exciting possibility of superconductivity in this system.

In order to further understand why presence of O-atoms in Ag or Au causes such an intense van Hove singularity, we find from the integration of the PDOS up to

$E_F$  that the total valence charge in O-atom varies from 4.4 to 4.6. Thus, the O-atom is almost neutral, with a small excess negative charge ( $2p^4$  is the valence configuration of oxygen). Its valency is remarkably smaller than the nominal valency of -2 for oxygen, for example, in stoichiometric oxides, where covalent bonding is predominant and Ag to O nearest neighbor ( $nn$ ) distance is  $\approx 2\text{\AA}$  [12]. On the other hand, in Ag/Au-O systems studied here, the  $nn$  distance between two O-atoms is substantially larger (e.g.  $2.84\text{\AA}$  for  $a_{eq} = 4.02\text{\AA}$ ) to have any covalent bonding. Rather, it is interesting to note that the van der Waals (vdW) diameter of the O-atom, i.e. the distance between two O-atoms where the minimum of the Lennard-Jones interaction potential occurs, is reported from different estimates to be in the range of  $2.8\text{\AA}$  [25] to  $3\text{\AA}$  [26]. Thus, based on the observations that the O-atoms are almost neutral and at a distance equivalent to their vdW diameter, the dominance of vdW bonding between O-atoms is expected.

In Fig. 1, the O  $2p$  states extend from  $E_F$  to -6 eV; it has a shoulder at -1.3 eV that arises mainly from the  $2p_{x,y}$  states, while the peak at  $E_F$  has similar contributions from all the three  $p$  components. Its noteworthy that in the -2.5 to -6 eV region (e.g. indicated by green horizontal arrow in Fig. 1(d)), the O  $2p$  PDOS tails out as almost flat with apparently low intensity, but in reality it constitutes about 20% of the total occupied PDOS. It has a similarity of shape with the Ag  $d$  states, with both exhibiting a minima at -4.5 eV (black arrow). Such tailing of the O  $2p$  PDOS is also observed for  $\text{Au}_{60}\text{O}_{40}$  and  $\text{Ag}_{30}\text{Au}_{30}\text{O}_{40}$  (Fig. 1(i,j)), indicating hybridization of the O  $2p$  states with the noble metal  $d$  states. The cohesive energies ( $E_{coh}$ ) of  $\text{Ag}_{60}\text{O}_{40}$  and  $\text{Au}_{60}\text{O}_{40}$  have been calculated by considering a  $2 \times 2 \times 2$  fcc supercell of 32 atoms with one particular configuration of 13 O-atoms using full potential linearized augmented plane wave (FP-LAPW) method [27]. The DOS shows the O  $2p$  related sharp peak at  $E_F$  (Fig. 5), which is of similar intensity as in Fig. 1(d). The PDOS shows also has the hump around -1.3 eV and the flat DOS region. However, the DOS in this case is highly structured; this is because here we have considered only one particular configuration of O-atoms that is repeated in space in the FP-LAPW method and thus it is not a fully disordered structure. The values of  $E_{coh}$  for  $\text{Ag}_{60}\text{O}_{40}$  and  $\text{Au}_{60}\text{O}_{40}$  are 2.8 eV/atom and 2.9 eV/atom, respectively. In comparison,  $E_{coh}$  for O in fcc structure with same lattice constant is much smaller 1.3 eV/atom. Thus, hybridization of O  $2p$  and the Ag/Au  $d$  states, as well as their cohesive energies indicate the importance of the noble metal matrix in providing the stability.

We have also considered O-atoms to be randomly distributed in octahedral and tetrahedral interstitial positions of Ag (Fig. 6(b,c)), since these have been reported in literature as possible sites that oxygen could occupy [4–6]. In both the interstitial positions, due to the close proximity of O and Ag atoms ( $2.04\text{\AA}$  for octahedral and

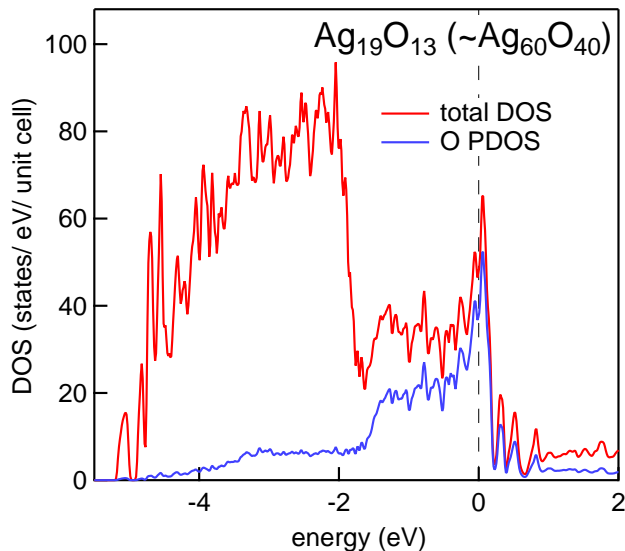


Figure 5: The total and oxygen density of states for  $\text{Ag}_{19}\text{O}_{13}$  calculated with a 32 atom fcc supercell using full potential linearized augmented plane wave method.

1.77 Å for tetrahedral sites), the Ag  $4d$ -O  $2p$  hybridization dominates and the Ag  $4d$  PDOS is largely modified. The O  $2p$  PDOS exists over a wide energy range of 10-12 eV, and does not have any peak at  $E_F$ . Nevertheless,  $n_F$  increases moderately with O-atom content (Fig. 6(a)). In contrast to Ag-O (Fig. 1), this is caused primarily by Ag  $4d$  and  $5s, p$  states rather than O  $2p$  states.

Very recently, room temperature superconductivity has been reported in 10 Å Ag NP in Au matrix, which we refer henceforth as Ag@Au nano-structure (NS)[19]. High temperature superconductivity could be achieved in materials with large  $n_F$  and high Debye temperature, however superconductivity in Ag@Au NS is surprising, since neither Ag or Au are superconducting. Although the authors do not mention about oxygen being present in their specimens, the EDAX data show presence of C and O  $K\alpha$  peaks at 0.28 and 0.53 keV, respectively. Ag NP are prone to oxidation[13, 14] and the following estimate provides an idea about possible oxygen content: in a 10 Å Ag NP, there are about 30 atoms. If a single O-atom layer is considered to fully cover this spherical NP, an estimate of the number of O-atoms considering these as hard spheres with atomic diameter of 1 Å will involve 400 O-atoms. However, the x-ray diffraction pattern shows that the Ag@Au NS has fcc structure with no extra phases[19]. This shows that the oxygen present does not form any of the known oxides of Ag that do not have fcc structure. Thus, O-atoms probably are present in disordered positions keeping the fcc structure unaffected and this justifies our approach of considering disordered positions for O-atoms in the

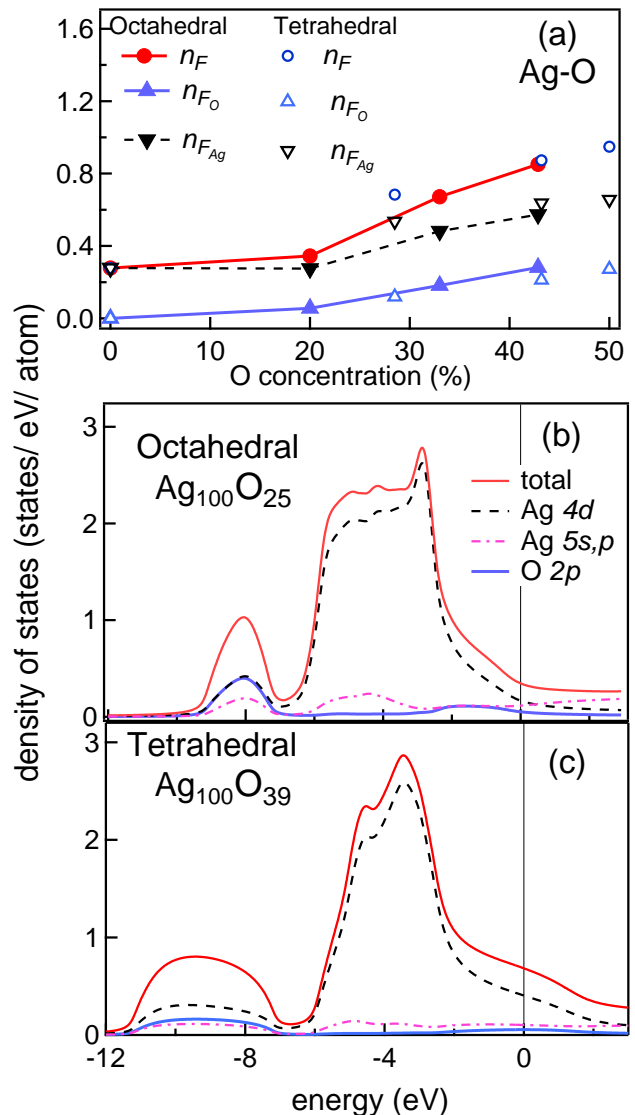


Figure 6: (a) The total DOS at  $E_F$  ( $n_F$ ) and the total Ag ( $n_{F_{Ag}}$ ) and O ( $n_{F_O}$ ) contributions to  $n_F$  for O-atoms in octahedral and tetrahedral interstitial positions, as a function of O-atom concentration. Total density of states, Ag  $4d$ , Ag  $5s, p$  and O  $2p$  PDOS for (b) octahedral  $\text{Ag}_{100}\text{O}_{25}$  and (c) tetrahedral  $\text{Ag}_{100}\text{O}_{39}$ , where disordered O-atoms and vacancies are considered in the interstitial sites.

bulk. We further point out that the O-atoms could be present in the Ag vacancy (*i.e.* substitutional) sites from the evidences provided by Shibata *et al.*[15], Oppenheim *et al.*[16] and Yue *et al.*[17], who establish presence of vacancies and O-atoms, their migration through the NP and complete alloying, particularly in small NP of size less than 46 Å (the Au NP in Ref. onlinecitePandey18 is 10 Å in size). Moreover, the DFT study by Crocombette *et al.* established that it is energetically favored for an oxygen-vacancy pair in Ag to transform to a substitutional O-atom[5]. On the basis

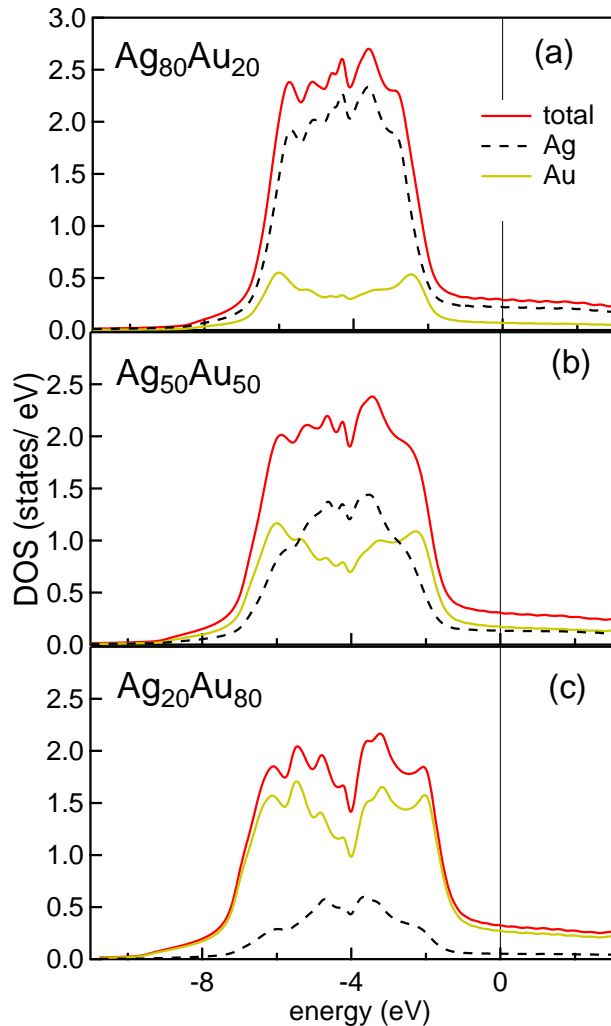


Figure 7: The total, Ag and Au density of states for (a)  $\text{Ag}_{80}\text{Au}_{20}$ , (b)  $\text{Ag}_{50}\text{Au}_{50}$  and (c)  $\text{Ag}_{20}\text{Au}_{80}$ . The position of the Ag  $4d$  and Au  $5d$  states remain essentially unchanged and their relative intensities vary proportionately with composition, with hardly any modification in the DOS of the  $s, p$  states at  $E_F$ .

of the above arguments, it is conceivable that O-atoms can form local regions of disordered Ag/Au-O with high oxygen concentration encompassing the Ag core and Au matrix, thus possibly forming a connected region of very high  $n_F$ . The quantum confinement effect that is well known for NP might further enhance  $n_F$ ; as has been shown for Ag NP of size less than  $15 \text{ \AA}$  by DFT[28]. The vdW bonding might be further enhanced in Ag@Au NS because it was shown from DFT that vdW bonding reduces their formation energy[29]. In an interesting work for sulfur protected Au NP, formation of Au-Au bonds that reduce the covalent contribution to Au-S bonds was demonstrated theoretically[30]. Another important point is that O-atoms have relatively large

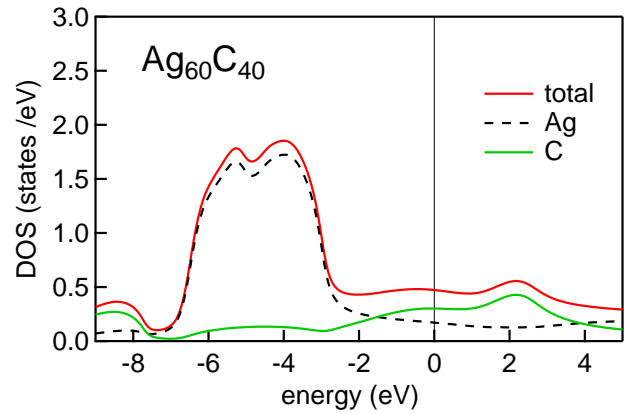


Figure 8: (a) The total, Ag and C density of states for  $\text{Ag}_{60}\text{C}_{40}$ , where C is in disordered substitutional positions. The calculation has been performed using optimized lattice constant ( $3.922 \text{ \AA}$ ). A peak in the C  $2p$  PDOS appears above  $E_F$  at  $2.2 \text{ eV}$ .

volume available in the substitutional position because of their smaller size. This could possibly lead to formation of polarons and/or rattling phonon modes, both of which are known to favor superconductivity. While we have argued above that presence of O-atoms in Ag vacancy positions might explain the results of Ref. [19], it is possible that alloying of Ag with Au (without any oxygen) would also provide some clue. So, in Fig. 7, we show DOS of site-disordered Ag-Au alloys from  $\text{Ag}_{90}\text{Au}_{10}$  to  $\text{Ag}_{10}\text{Au}_{90}$ , but unfortunately, we do not find any enhancement of  $n_F$  nor any transfer of charge from Ag to Au. We have also considered disordered carbon in Ag (Ag-C), as carbon is abundantly present in the EDAX signal of Ag@Au NS[19]. The DOS of  $\text{Ag}_{60}\text{C}_{40}$  in Fig. 8 does not show any peak at  $E_F$  and  $n_F (= 0.47 \text{ states/eV/atom})$ , although larger than Ag, is considerably less compared to  $\text{Ag}_{60}\text{O}_{40}$ .

### Conclusion:

To conclude, incorporation of O-atoms and formation of continuous possibly superconducting regions of Ag-Au-O between the probe leads at some step(s) of the NS fabrication that involves complicated chemical reactions is probably uncontrolled at present. This is presumably a reason for very large variation of  $T_C$  ( $140$  to  $320 \text{ K}$ ) in Ref. [19]. We hope that our work will motivate new focused experiments on Ag@Au NS, the first step would be to microscopically investigate the distribution of the O-atoms.

The novelty of our work is to point out the prospect of superconductivity related to van Hove singularity at the Fermi level if van der Waals bonded oxygen can be stabilized in a noble metal matrix.

### Acknowledgments:

We thank the Computer Centre of Raja Ramanna Centre for Advanced Technology, Indore for providing the computational facility. A.C. thanks P.A. Naik and A. Banerjee for support and encouragement.

- 
- [1] E. H. Baker, J. K. Johnstone, *Nature* **205**, 66 (1965).  
 [2] P. A. Gravil, D. M. Bird, J. A. White, *Phys. Rev. Lett.* **77**, 3933 (1996).  
 [3] X. Bao *et al.*, *Surf. Sci.* **284**, 14 (1993).  
 [4] M. E. Eberhart, M. M. Donovan, R. A. Outlaw, *Phys. Rev. B* **46**, 12744 (1992).  
 [5] J.-P. Crocombette, H. de Monestrol, F. Willaime, *Phys. Rev. B* **66**, 024114 (2002).  
 [6] J. K. Baird, T. R. King, C. Stein, *J. Phys. Chem. Sol.* **60**, 891 (1999).  
 [7] A. J. Nagy, G. Mestl, R. Schlögl, *J. Catal.* **188**, 58 (1999).  
 [8] W.-X. Li, C. Stampfl, M. Scheffler *Phys. Rev. Lett.* **90**, 256102 (2003).  
 [9] W. H. A. Thijssen *et al.*, *Phys. Rev. Lett.* **96**, 026806 (2006).  
 [10] O. Bourgeois, A. Frydman, R.C. Dynes, *Phys. Rev. Lett.* **88**, 186403 (2002).  
 [11] Y. Quan, W. E. Pickett, *Phys. Rev. B* **91**, 035121 (2015).  
 [12] J.P. Allen, D.O. Scanlon, and G.W. Watson, *Phys. Rev. B* **84**, 115141 (2011).  
 [13] C. Shankar *et al.*, *Nanotech.* **23**, 245704 (2012).  
 [14] I. S.- Šloufová *et al.*, *Langmuir* **20**, 3407 (2004).  
 [15] T. Shibata *et al.*, *J. Am. Chem. Soc.* **124**, 11989 (2002).  
 [16] I. C. Oppenheim *et al.*, *Science* **254**, 687 (1991).  
 [17] Y. Yue *et al.*, *Nature Comm.* **7**, 12251 (2016).  
 [18] H. Ebert, D. Ködderitzsch, J. Minár, *Rep. Prog. Phys.* **74**, 096501 (2011).  
 [19] D. K. Thapa and A. Pandey, arXiv:1807.08572  
 [20] J. P. Perdew, K. Burke, M. Ernzerhof, *Phys. Rev. Lett.* **77**, 3865 (1996).  
 [21] H. Ebert, D. Ködderitzsch, J. Minár, *Rep. Prog. Phys.* **74**, 096501 (2011).  
 [22] C. C. Tsuei *et al.*, *Phys. Rev. Lett.* **65**, 2724 (1990).  
 [23] G. Li *et al.*, *Nature Phys.* **6**, 109 (2010).  
 [24] Y. Cao *et al.*, *Nature* **556**, 43 (2018).  
 [25] L. Pauling, *The Nature of the Chemical Bond*, Ithaca: Cornell Univ., (1960)  
 [26] A. Bondi, *J. Phys. Chem.* **68**, 441 (1964).  
 [27] P. Blaha *et al.*, WIEN2k, (Karlheinz Schwarz, Techn. Universität Wien, Austria), 2001. ISBN 3-9501031-1-2.  
 [28] F.D. Kiss, R. Miotto, A.C. Ferraz, *Nanotechnol.* **22**, 275708 (2011).  
 [29] R. Miotto *et al.*, ICQNM 2014 : The Eighth International Conference on Quantum, Nano Bio, and Micro Technologies, p.28 (2014).  
 [30] J. R. Reimers *et al.*, *Proc. Natl. Acad. Sci. U.S.A.* **113**, E1424 (2016).